Available online at www.sciencedirect.com
SCIENCE DIRECT
Diamond & Related Materials 14 (2005) 113–120
DIAMOND AND RELATED MATERIALS
www.elsevier.com/locate/diamond

Estimation of parameters in thermal-field emission from diamond

D.G. Walker[a], C.T. Harris[a], T.S. Fisher[b,*], J.L. Davidson[c]

[a]Department of Mechanical Engineering, Vanderbilt University, Nashville, TN, United States
[b]School of Mechanical Engineering and Birck Nanotechnology Center, Purdue University, West Lafayette, IN 47907-2040, United States
[c]Department of Electrical Engineering, Vanderbilt University, Nashville, TN, United States

Received 24 October 2003; received in revised form 14 July 2004; accepted 22 July 2004
Available online 11 September 2004

Abstract

This paper reports on the behavior of electron field emission from diamond thin films at elevated temperatures. The study is motivated by the possibility of using these structures in high temperature electronics or direct energy conversion processes. Three diamond samples were tested: nanocrystalline diamond, crowned diamond tips, and peaked diamond tips. All samples displayed moderately efficient field emission characteristics. For each of the samples, the onset of field emission decreased as the sample temperature increased. Temperature effects, interpreted through advanced parameter estimation techniques, were shown to have a small influence on the estimated work function between 300 and 700 K, except for the peaked tip sample, whose estimated work function became very large at the highest temperature. Emission areas were also estimated and revealed similar trends to that of work function.

PACS: 85.45.Db
Keywords: Thermal field emission; Diamond film

1. Introduction

Polycrystalline diamond films can exhibit outstanding field emission properties with low turn on fields and high current densities. The precise mechanism(s) responsible for this behavior remain unclear, but most prior studies attribute at least some of the behavior to the presence of small-scale geometric features that serve as sites of local electric field enhancement [1]. Numerous studies [2–8] have highlighted the shortcomings of basic Fowler-Nordheim theory [9] applied to emission from small surface features. In such cases, the meaning of the three primary Fowler-Nordheim parameters—work function, area, and field enhancement factor—can become obscured. In the present work, we employ an emission model that includes non-planar effects to explain observed field emission from polycrystalline diamond films at elevated temperatures. Thermal effects are included in the models and provide an important additional degree of freedom in interpreting field emission behavior via advanced parameter estimation techniques.

A variety of diamond films show strongly enhanced field emission properties that can be demonstrated reproducibly. Several possible mechanisms have been proposed to explain such outstanding behavior. Wang et al. [10] observed emission from the region between grains in polycrystalline diamond films. Geiss et al. [11] described a theory involving internal emission from a metallic electrode into the cathode's conduction band. Recently, nanocrystalline films [12–15] have shown excellent field emission properties. Diamond tip arrays also appear to be promising candidates for electron field emission devices because of the field enhancement produced by their geometry [16,17]. This effect occurs due to a deformation of the potential field, which enhances the local electric field and enables emission of electrons at low applied voltages.

Several recent studies have reported significant effects of temperature on field emission from diamond [18–22]. Sugino et al. [18] observed a substantial decrease in turn-

* Corresponding author. Tel.: +1 765 494 5627; fax: +1 765 494 0539.
E-mail address: tsfisher@purdue.edu (T.S. Fisher).

0925-9635/$ - see front matter © 2004 Elsevier B.V. All rights reserved.
doi:10.1016/j.diamond.2004.07.013

on voltage as temperature increased from 20 to 200 °C for phosphorus-doped films. Koch et al. [19, 20] also observed such an effect at higher temperatures (up to 950 °C) for nitrogen-doped films. At lower temperatures, Chen and Lue [21] observed a significant decrease in emission from room temperature to 100 K for boron-doped films. The strong temperature effects observed in these studies suggests that temperature variation may be useful in clarifying emission mechanisms and unknown parameters (such as work functions, emission areas, and geometric feature sizes) in field emission materials.

The present work seeks to elucidate emission mechanisms from diamond films by considering geometric and thermal effects in models that are used to interpret experimental observations. Rigorous estimation techniques are employed to determine values of unknown parameters, and experimental variations are included explicitly in the process. The following section describes the development and implementation of emission models and parameter estimation techniques. The subsequent section describes experimental implementation. Section 4 presents experimental observations and comparisons with theory through parameter estimation. The final section summarizes with several conclusions derived from the work.

2. Theoretical formulation

The outstanding field emission properties of many cathode materials are a consequence of localized field enhancement from extremely small geometric features. Often, Fowler-Nordheim (FN) theory of field emission has been applied to the analysis of tip-like emitters due to its simplicity (and a "universal" model based on FN theory has even been proposed for emission from carbon nanotubes [23]). However, FN theory makes several simplifications to arrive at an analytic solution whose validity for predicting emission from sharp objects and emission at elevated temperatures is questionable. A common remedy for reconciling the difference between planar field emission (presumed by FN theory) and emission from small protrusions involves the use of a field enhancement factor (β) that linearizes the highly curved field near the location of emission. The hazards of such an approach for simulating field emission from CNTs has been documented recently [8], and earlier studies have shown the significant limitations of FN theory for other types of tip emitters [2,4,7]. In addition, recent studies have shown that the FN linearization can cause signification deviation in the predicted energy distributions of emitted electrons [24,25].

Prior studies [26–28] have shown that a floating sphere model can approximate, to reasonable accuracy, the local electric field near the surface of a field emitter with a sharp tip. The model begins with a description of electron potential surrounding a conducting sphere of radius a within a uniform electric field, F [29, pp. 60–62]. The sphere's surface potential can be matched approximately to that of the planar cathode at a distance L from the sphere's center (see Fig. 1) via superposition of a point source of strength FLa located at the sphere's center. Thus, setting the magnitude of the cathode and sphere surface potentials to zero, the potential becomes, in spherical-polar coordinates with image potential,

$$\phi(r,\theta) = -qF\left(r - \frac{a^3}{r^2}\right)\cos\theta + qFL\left(\frac{a}{r} - 1\right) - \frac{q^2 a(K-1)}{8\pi\epsilon_0(r^2-a^2)(K+1)}, \quad (1)$$

where r is the radial coordinate measured from the sphere's center, θ is the polar angle, F is the macroscopic electric field, q is the elementary electron charge, ϵ_0 is the permittivity of vacuum, and K is the emitter's dielectric constant. The macroscopic field can be expressed in terms of the applied voltage V and cathode-anode separation distance d as $F=V/d$.

For tunneling calculations, the foregoing potential field is approximated by a one-dimensional potential along the axis $\theta=0$ [8]. The WKB tunneling approximation [30, pp. 229–233] is used to evaluate the tunneling coeficient $D(W)$

$$D(W) = \int_{x_1}^{x_2} \sqrt{\frac{8m}{\hbar^2}|\phi_0(x) - W|}\,\mathrm{d}x \quad (2)$$

where x is the linear coordinate measured from the tip apex along the axis $\theta=0$, ϕ_0 is the potential along this axis, and $W=mv_x^2/2$ is the energy associated with momentum in the tunneling direction. The limits of integration x_1 and x_2 are the roots of $W-\phi_0$. These roots can be determined by

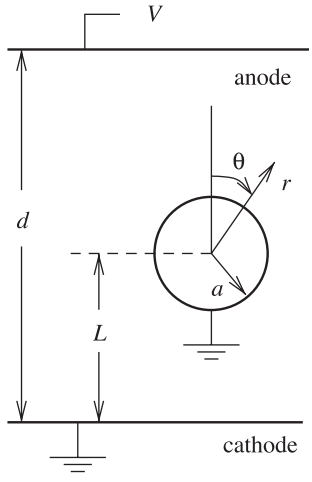

Fig. 1. Coordinates and dimension definitions used in the calculation of potentials.

expressing $W-\phi_0=0$ as a polynomial in a normalized coordinate $x' = 1+x/a$

$$0 = Fqax'^5 + (W + FqL)x'^4 - Fq(L + a)x'^3 + \left[\frac{q^2k_1}{2a} - Fq(L + a) - W\right]x'^2 + FqLx' + Fqa \quad (3)$$

where $k_1=(4\pi\epsilon_0)^{-1}$. Evaluation of the transmission coefficient in Eq. (2) is aided by precalculation of the maximum potential, ϕ_{max}, which is given by the real, positive root of the equation

$$0 = Fqax'^7 + Fq(L - 2a)x'^5 + \left(2Fqa - \frac{q^2k_1}{a}\right)x'^4 + Fq(a - 2L)x'^3 - 4Fqax'^2 + FqLx' + 2Fqa. \quad (4)$$

Electron emission also depends on the number of electrons available for emission with sufficient energy to tunnel. Following Good and Müller [31], the electron supply function is taken as

$$N(W)\mathrm{d}W = \frac{4\pi mkT}{h^3}\ln\left[1 + \exp\left(-\frac{W - \xi}{kT}\right)\right]\mathrm{d}W, \quad (5)$$

where m is the mass of an electron, k is Boltzmann's constant, and T is emitter temperature. Temperature-dependent emission is introduced through the supply function. Electron emission is found by integrating the product of Eqs. (5) and (2).

$$I = Aq\int_{-W_a}^{\infty} D(W)N(W)\mathrm{d}W, \quad (6)$$

where A is the emission area and $-W_a$ is the energy at the bottom of the conduction band.

2.1. Parameter estimation

Parameter extraction is usually performed by curve fitting a model to experimental data. In the case of the FN equation, the solution can be cast in terms of a line whose slope and intercept can be resolved into the parameters of interest, namely the enhancement factor β and work function ϕ. Because an analytic solution for the emission current is not forthcoming in the present context, the forward model (emission current) must be solved by numerical integration. As such, estimation of model parameters becomes difficult. Further, noise inherent to experimental measurements introduces uncertainty in parameter estimates, and this noise should be characterized. Inverse methods [32] and parameter estimation techniques [33] have been developed to extract model parameters while including information about random noise.

Estimation of model parameters begins by considering a least-squares minimization of the residual between predicted model outcomes and measurements. The objective is given as

$$S = [\boldsymbol{I} - \eta(\gamma)]^T\boldsymbol{\Phi}^{-1}[\boldsymbol{I} - \eta(\gamma)], \quad (7)$$

where the $\boldsymbol{I}$ vector contains the measured current, the $\eta(\gamma)$ vector contains the model prediction corresponding to the measurements as a function of the model parameters, γ and $\boldsymbol{\Phi}$ is the covariance matrix of measurement errors. In the present work, $\gamma=\{a, \phi, A\}$, and $\boldsymbol{\Phi}$ contains the standard deviation of the measurement error along its diagonal. Errors are generally field-dependent and increase with applied bias V. The parameter estimation procedure has been used previously [34] for estimation of field emission parameters using a different forward emission model.Estimation of the parameter vector follows from a non-linear correction form

$$\tilde{\gamma}_{i+1} = \tilde{\gamma}_i + \Delta\gamma; \Delta\gamma = \frac{\mathbf{X}^T\boldsymbol{\Phi}^{-1}[\boldsymbol{I} - \eta(\tilde{\gamma}_i)]}{\mathbf{X}^T\boldsymbol{\Phi}^{-1}\mathbf{X}}, \quad (8)$$

where the subscript indicates the iteration number and the tilde indicates that the vector represents an estimate. The sensitivity matrix $\mathbf{X}$ contains the derivatives of the prediction with respect to the parameters. Because the forward model is not analytic, a finite difference is used such that

$$\mathbf{X} = \frac{\partial\eta(\gamma)}{\partial\gamma} \approx \frac{\eta(\gamma + \delta\gamma) - \eta(\gamma)}{\delta\gamma}. \quad (9)$$

The iteration repeats until the objective (Eq. (7)) is of the order of the measurement noise.

3. Experimental procedure

Three different samples were fabricated and tested in this work. The first sample was a nanocrystalline film fabricated according to the protocol described by Zhou et al. [12]. The film was deposited on a silicon substrate (100 orientation) to a thickness of approximately 0.5 μm. The other two samples possessed molded pyramidal tip features and were prepared as described by Kang et al. [35]. Two different silicon molds were employed with base pyramid dimensions of 2 and 3 μm, respectively. For the 2-μm base, each inverted pyramidal mold ended with a single sharp-pointed peak. For the 3-μm base, the silicon mold was over-etched such that the inverted mold ended in a four-sided crown, instead of a single tip. Hereafter, the two samples are identified as 'peaked' and 'crowned', respectively.

The crowned and peaked diamond samples are shown in Fig. 2. After deposition into the inverted silicon molds, the exposed surface was brazed to a planar molybdenum substrate of 2.5-mm thickness. The silicon mold was then removed completely by etching in KOH. The samples were mounted on a heated stage in vacuum for emission testing.

A Hewlett Packard 6621A DC power supply provided and maintained heat input. Temperature measurement, via K-type thermocouples, was recorded on the top surface of each sample, and the output signal was monitored using a Fluke model 52-II thermocouple thermometer. A floating zirconium probe was implemented as the biasing anode.

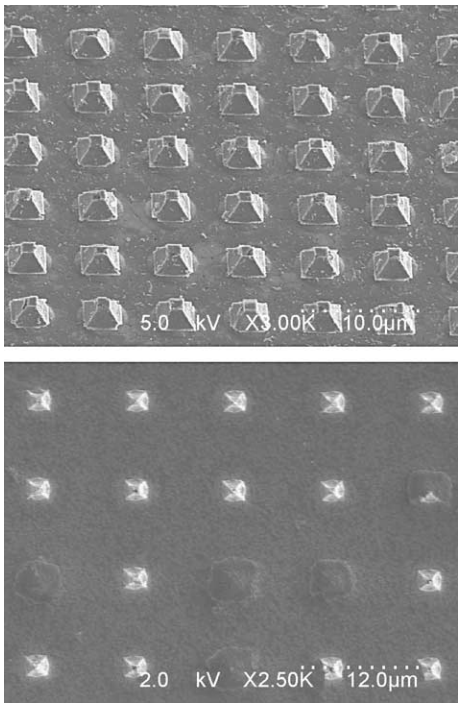

Fig. 2. Sem image of diamond tips; (a) crowned diamond microtips, (b) peaked diamond microtips.

Vacuum gap positioning was controlled in the vertical direction using a Burliegh 1700–25 inchworm motor and 6000 ULN controller. The vacuum gap was 10 μm for each test. A voltage bias ranging from 0 to 1000V was applied across each of the samples under a typical vacuum chamber pressure of 1×10^{-7} Torr. This procedure was repeated for various temperature settings in the range 300–700 K.

4. Results

Plots of field emission current as a function of applied voltage for the nanocrystalline diamond film are shown in Fig. 3. The results indicate a room-temperature emission turn-on field (i.e., the field at which current exceeds 1 μA) of approximately 65 V/μm. At T=500 K, the turn-on voltage decreases to 55 V/μm. However, prior study shows turn-on voltages for nanocrystalline diamond in the range of 3–5 V/μm [12]. The larger turn-on fields observed in the present work could be the result of differences in grain structure. The inset of Fig. 3 shows the Fowler-Nordheim plot for the nanocrystalline sample in which each data set exhibits approximately the same slope. The similar slopes of the samples indicate a relatively unchanging field enhancement factor β (assuming a constant work function), which is estimated to be 1.56×105 and 1.25×105 cm^{-1} for the respective temperatures of 300 and 500 K, assuming a work function of 4.5 eV. These values are similar to those estimated from other experiments [13]. As previously mentioned, the nanocrystalline diamond film produced higher currents for a given voltage as the sample temperature increased. This result can be attributed, in part, to the supply function's temperature dependence wherein higher temperatures produce increased supply of electrons available for emission, resulting in larger currents.

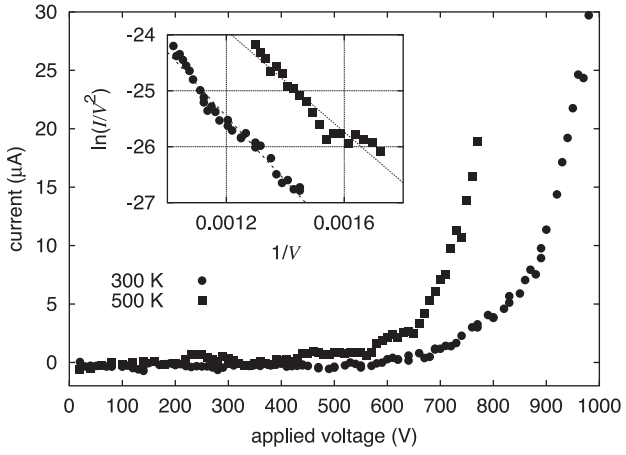

Fig. 3. Current–voltage behavior of the nanocrystalline diamond thin film.

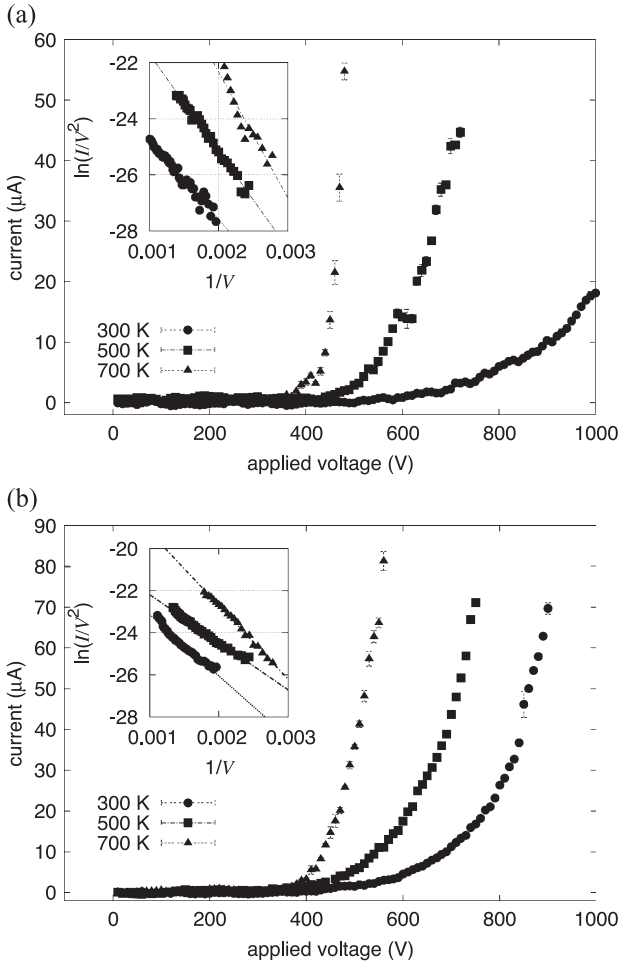

Fig. 4. Current–voltage behavior of diamond-tip emitters; (a) peaked device, (b) crowned device.

Fig. 4 displays the current–voltage characteristics of the peaked and crowned diamond tip samples. The emission characteristics of these samples are similar. Fowler-Nordheim (FN) plots for the two diamond tip devices are shown in the insets of Fig. 4. These plots confirm that both devices exhibit field emission behavior. Using isothermal FN theory, estimated values of field enhancement factor β for the crowned sample range from 7.63×104 to 2.91×105cm^{-1}. Estimated values of β for the peaked-tip sample range from 2.50×105 to 3.42×105 cm^{-1}. Crowned tips and peaked tips follow the same thermal trend as the nanocrystalline films, as the FN lines shift to the right with increasing temperature, while generally maintaining a relatively constant slope.

Improved insight into temperature effects on field emission can be obtained from examining estimates of parameters inherent to the non-analytic model of Eq. (6). The parameters of interest include work function ϕ, effective emission area A, tip radius a, and tip height L. The field enhancement factor in the FN formulation is inversely proportional to the tip radius and proportional to tip height. Because this model contains physical geometric quantities instead of fitting parameters, more reliable estimates for work function and effective emission area can be obtained. The following paragraphs discuss the results of this model in terms of the interdependencies among the estimated physical parameters, highlight the results among different parameter types, and illustrate the temperature dependence of the estimated parameters for the various samples under study.

For the nanocrystalline film sample, estimates of work function are shown in Fig. 5 as a function of tip radius. Because of the correlation of parameters, only effective area and work function were estimated simultaneously. Consequently, the tip radius was swept through a range of values for each data set, and the tip height was held constant at 0.5 μm. The estimates do not definitively indicate the work function. Instead, they provide a bound on the tip size based on physical arguments. Because the work function is expected to exist in the range of 3.2–5.1 eV [36], the estimated tip radius

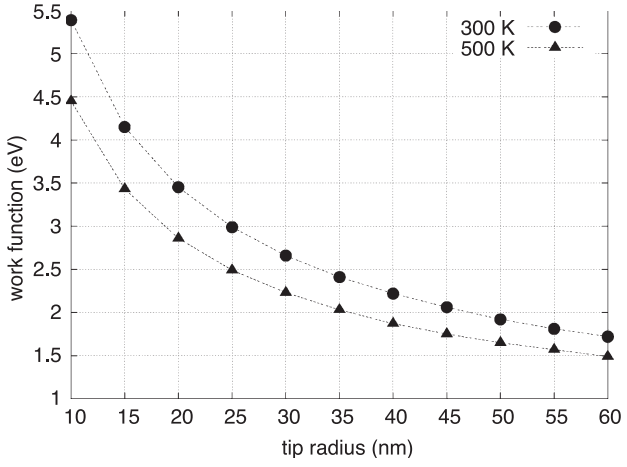

Fig. 5. Estimate of work function for nanocrystalline thin film.

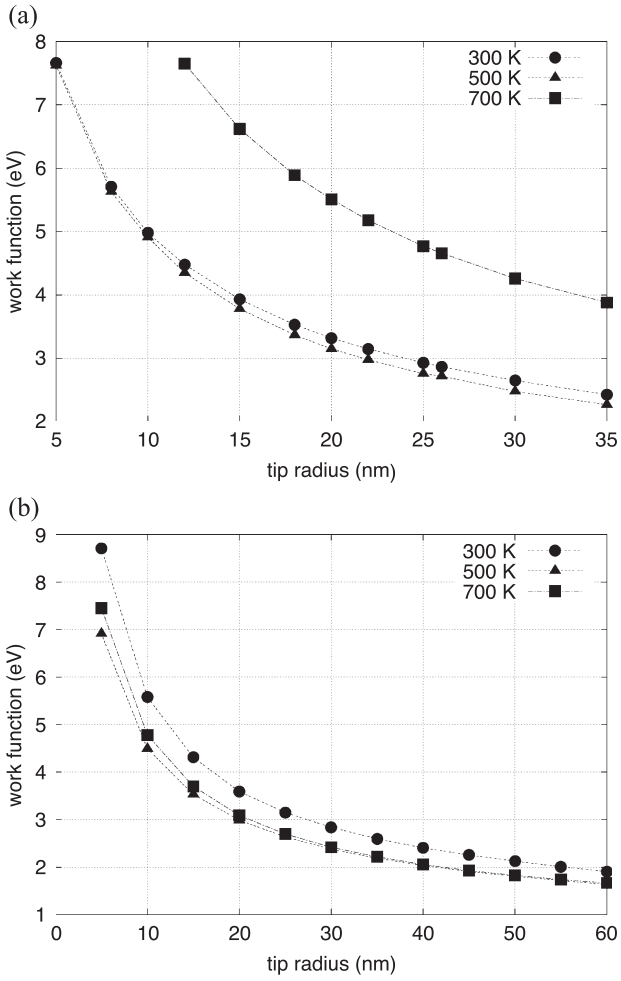

Fig. 6. Estimates of work function for (a) peaked sample and (b) crowned sample.

falls between 10 and 25 nm. Interestingly, the estimated work function decreases by approximately 0.5 eV as temperature increases from 300 to 500 K. Higher temperatures were not tested with this sample due to catastrophic arcing failure. The area estimates were found to be ~10^{-4} μm^2 for both temperatures. Although the value increased slightly for increasing tip radii, the increase was negligible.

Fig. 6 shows estimated work functions of both the peaked tip sample and the crowned sample for varying emitter radii. Both show the same trends and place the tip radius in the range of 10–25 nm based on expected work function values. Further, these values are consistent with estimates of the nanocrystalline diamond sample in Fig. 5.

For the peaked sample, the work function estimates at the lower two temperatures are similar for all emitter radii. However, for the highest temperature, the estimated work function increases dramatically. This increase is apparent in the I–V curve of Fig. 4, where a kink appears just after device turn-on. Considering the FN plot in the inset, two distinct FN slopes are apparent on either side of this feature. The estimation procedure, which cannot resolve two slopes, is weighted toward the slope of larger magnitude and thus

predicts a higher work function. For the crowned sample in Fig. 6, the estimated work function decreases between 300 and 500K and then remains relatively the same between 500 and 700 K. This behavior at lower temperatures is consistent with that of the nanocrystalline film.

Temperature also affects a strong change in emission area, as shown in Fig. 7. At lower temperatures, estimated area increases for the peaked sample and decreases for the crowned sample. The former result seems intuitive, as the relatively constant work function observed in Fig. 6a would require larger areas to produce markedly higher currents, as observed in Fig. 4a. The latter observation is less obvious but is the result of the decrease in work function between 300 and 500 K. Apparently, this decrease in work function occurs over relatively small regions of the emitter sample, and these regions then dominate the emission characteristics. At the highest temperatures, the emission area increases significantly for both samples and may be the result of improved conduction in the emitter materials.

The preceding results at the highest temperatures are generally consistent with those of Koch et al. [20] and indicate an increase in emission area at these temperatures.

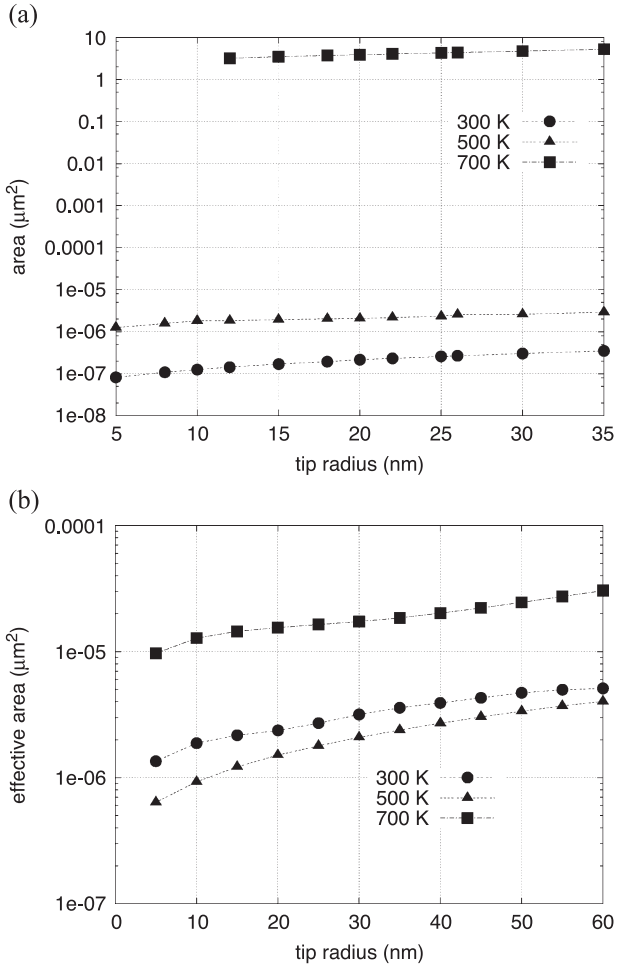

Fig. 7. Estimates of effective emission area for (a) peaked sample and (b) crowned sample.

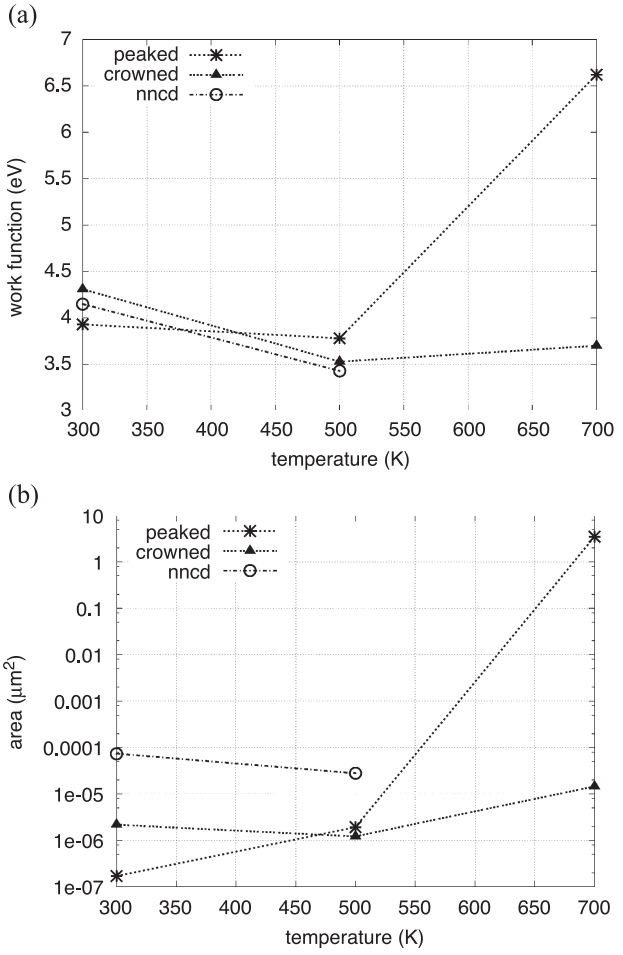

Fig. 8. Temperature dependence of (a) work function and (b) effective area.

To highlight temperature effects, estimates at a tip radius of 15 nm were selected for further investigation. Fig. 8 shows results for work function and emission area in terms of temperature explicitly. The estimated work functions for all samples exhibit small decreases with increasing temperature at low temperatures, but the work function for the peaked sample increases markedly between 500 and 700 K. A possible explanation for this behavior, and one supported by the results of Koch et al. [20], is that hydrogen desorption occurs in this temperature range, causing an increase in diamond's electron afinity and therefore effective work function. Emission area plotted in Fig. 8(b) as a function of temperature on a logarithmic-linear scale indicates relative stability in emission area at low temperatures but a significant increase in area at high temperatures. These results are consistent with observed phosphor screen images taken by Koch et al. [20] in which isolated the emission locations are seen at low and moderate temperatures, but nearly uniformly emission is observed at high temperatures. We note that a rigorous physical explanation of this behavior has not yet been proposed. However, an increase in electron mobility in the bulk emitter material and on its surface is a likely contributor to this behavior.

5. Conclusions

The present study presents temperature-dependent field emission measurements of nanocrystalline diamond and two samples of geometrically enhanced 9 polycrystalline diamond. For each sample, the turn-on voltage decreased as temperature increased, which is consistent with other observations. This result is explained by considering a temperature dependent supply function. In this case more electrons are available for emission. However, estimates indicate that the work function can increase with temperature, which would effectively decrease the current of an emitter if this were the only effect. Estimates also indicate that effective area increases with temperature, which is also consistent with other observations. The net result is significantly larger currents at elevated temperatures. At lower temperatures, from 300 to 500 K, the increase is likely due to an increase in the supply function. At higher temperatures, 500–700 K, the increase in supply function alone does not account for the observed increase in current. Surface termination likely plays a significant role by allowing many more emission sites to become active. This suggests that the increase in current occurs suddenly near a particular temperature. More tests are warranted to investigate thermally enhanced field emission.

Acknowledgments

The authors gratefully acknowledge funding support through an NSF CAREER grant, an NSF NIRT grant, and DARPA/ARO's Palm Power program.

References

[1] R.G. Forbes, Low-macroscopic-field electron emission from carbon films and other electrically nanostructred heterogeneous materials: hypothesis about emission mechanism, Solid-State Electronics 45 (2001) 779–808.
[2] J. He, P.H. Cutler, N.M. Miskovsky, T.E. Feuchtwang, Derivation of the image interaction for non-planar pointed emitter geometries: Application to field emission I–V characteristics, Surface Science 246 (1991) 348–364.
[3] J. He, P.H. Cutler, N.M. Miskovsky, Generalization of Fowler-Nordheim field emission theory for nonplanar metal emitters, Applied Physics Letters 59 (1991) 1644–1646.
[4] P.H. Cutler, J. He, N.M. Miskovsky, Theory of electron emission in high fields from atomically sharp emitters: validity of the Fowler-Nordheim equation, Journal of Vacuum Science & Technology B 11 (1993) 387–391.
[5] P.H. Cutler, J. He, N.M. Miskovsky, B. Weiss, T.E. Sullivan, Theory of electron emission in high fields from atomically sharp emitters: validity of the Fowler-Nordheim equation, Progress in Surface Science 42 (1993) 169–185.
[6] K.L. Jensen, A.K. Ganguly, Numerical simulation of field emission and tunneling: a comparison of the wigner function and transmission coefficient approaches, Journal of Applied Physics 73 (9) (1993 May) 4409–4427.
[7] K.L. Jensen, P. Mukhopadhyay-Phillips, E.G. Zaidman, K. Nguyen, M.A. Kodis, L. Malsawma, C. Hor, Electron emission from a single spindt-type filed emitter: comparison of theory with experiment, Applied Surface Science 111 (1997) 204–212.
[8] J.-M. Bonard, K.A. Dean, B.F. Coll, C. Klinke, Field emission of individual carbon nanotubes in the scanning electron microscope, Physical Review Letters 89 (19) (2002 November) 7602.
[9] R.H. Fowler, L.W. Nordheim, Field emission from metallic surfaces, Proceedings of the Royal Society. A 119 (1928) 173–181.
[10] C.T. Wang, A. Garcia, D.C. Ingram, M. Lak, M.E. Kordesch, Cold field emission from CVD diamond films observed in emission electron microscopy, Electronics Letters 27 (1991) 1459–1461.
[11] M.W. Geiss, J.C. Twichell, T.M. Lyszczarz, Diamond emitters fabrication and theory, Journal of Vacuum Science & Technology. B 14 (1996) 2060–2067.
[12] D. Zhou, A.R. Krauss, L.C. Qin, T.G. McCauley, D.M. Gruen, T.D. Corrigan, R.P.H. Chang, H. Gnaser, Synthesis and electron field emission of nanocrystalline diamond thin films grown from N_2/CH_4 microwave plasmas, Journal of Applied Physics 82 (1997) 4546–4550.
[13] K. Okano, T. Yamada, A. Sawabe, S. Koizumi, J. Itoh, G.A.J. Amaratunga, Metal-insulator-vacuum type electron emission from N-containing chemical vapor deposited diamond, Applied Physics Letters 79 (2001) 275–277.
[14] B.D. Yu, Y. Miyamoto, Efficient n-type doping of diamond using surfactant-mediated epitaxial growth, Applied Physics Letters 76 (2000) 976–978.
[15] V.I. Merkulov, D.H. Lowndes, Field-emission studies of smooth and nanostructured carbon films, Applied Physics Letters 57 (1999) 1228–1230.
[16] V.T. Binh, S.T. Purcell, Field emission from nanotips, Applied Surface Science 111 (1997) 157–164.
[17] W.P. Kang, T.S. Fisher, J.L. Davidson, Diamond microemitters—the new frontier of electron field emissions and beyond, New Diamond and Frontier Carbon Technology 11 (2) (2001) 129–146.
[18] T. Sugino, K. Kuriyama, C. Kimura, Y. Yokota, S. Kawasaki, S. Shirafuji, Field emission from phosphorus-doped polycrystalline diamond films, Journal of Applied Physics 86 (1999) 4635–4642.
[19] F.A.M. Koch, J.M. Garguilo, R.J. Nemanich, Imaging electron emission from diamond film surfaces: N-doped diamond vs. nanostructured diamond, Diamond and Related Materials 10 (2001) 1714–1718.
[20] F.A.M. Koch, J.M. Garguilo, B. Brown, R.J. Nemanich, Enhanced low-temperature thermionic field emission for surface-treated n-doped diamond films, Diamond and Related Materials 11 (2002) 774–779.
[21] S.-Y. Chen, J.-T. Lue, Temperature dependence of surface band bending and field emission for boron-doped diamond and diamond-like films, New Journal of Physics 4 (2002) 79.1–79.7.
[22] S.H. Shin, T.S. Fisher, D.G. Walker, A.M. Strauss, J.L. Davidson, High-temperature electron emission from diamond films, Journal of Vacuum Science & Technology. B 21 (2003) 587–592.
[23] D.Y. Zhang, G.Y. Zhang, S. Liu, T. Sakurai, E.G. Wang, Universal field-emission model for carbon nanotubes on a metal tip, Applied Physics Letters 80 (3) (2002) 506–508.
[24] T.S. Fisher, Influence of nanoscale geometry on the thermodynamics of electron field emission, Applied Physics Letters 79 (22) (2001 November) 3699–3701.
[25] T.S. Fisher, D.G. Walker, Thermal and electrical energy transport and conversion in nanoscale electron field emission processes, Journal of Heat Transfer 124 (2002 October) 954–962.
[26] T. Utsumi, Keynote address vacuum microelectronics: What's new and exciting, IEEE Transactions on Electron Devices 38 (10) (1991) 2276–2283.
[27] K.L. Jensen, E.G. Zaidman, M.A. Kodis, B. Goplen, D.N. Smithe, Analytical and seminumerical models for gated field emitter arrays: I. Theory, Journal of Vacuum Science & Technology. B 14 (3) (1996) 1942–1946.

[28] G.E. Vibrans, Vacuum voltage breakdown as a thermal instability of the emitting protrusion, Journal of Applied Physics 35 (10) (1964) 2855–2857.
[29] J.D. Jackson, Classical Electrodynamics, 2nd ed., Wiley and Sons, New York, 1975.
[30] R.W. Robinett, Quantum Mechanics: Classical Results, Modern Systems, and Visualized Examples, Oxford University Press, New York, 1997.
[31] R.H. Good, E.W. Müller, Field emission, in: S. Flugge (Ed.), Encyclopedia of Physics, vol. 21, Springer-Verlag, Berlin, 1956, pp. 176–231.
[32] A.N. Tikhonov, V.Y. Arsenin, Solutions of Ill-Posed Problems, V.H. Winston and Sons, Washington, DC, 1977.
[33] James V. Beck, Kenneth J. Arnold, Parameter Estimation in Engineering and Science, John Wiley & Sons, 1977.
[34] D.G. Walker, T.S. Fisher, J.L. Davidson, W.P. Kang, Parameter estimation for electron field emission, Proceedings of the Applied Diamond Conference/Frontiers in Carbon Technology, Auburn, Al, August, 2001.
[35] W.P. Kang, J.L. Davidson, M. Howell, B. Bhuva, D.L. Kinser, D.V. Kerns, Q. Li, J.F. Xu, Micropatterned polycrystalline diamond field emitter vacuum diode arrays, Journal of Vacuum Science & Technology. B 14 (1996) 2068–2071.
[36] P. Abbott, E.D. Sosa, D.E. Golden, Effect of average grain size on the work function of diamond films, Applied Physics Letters 79 (17) (2001) 2835–2837.